analytical chemistry

Article

pubs.acs.org/ac

A Fully Unsupervised Compartment-on-Demand Platform for Precise Nanoliter Assays of Time-Dependent Steady-State Enzyme Kinetics and Inhibition

Fabrice Gielen,[†] Liisa van Vliet,[†] Bartosz T. Koprowski,[§] Sean R. A. Devenish,[†] Martin Fischlechner,[†,⊥] Joshua B. Edel,[‡] Xize Niu,*[,∥,⊥] Andrew J. deMello,*[,§] and Florian Hollfelder*[,†]

[†]Department of Biochemistry, University of Cambridge, 80 Tennis Court Road, CB2 1GA, United Kingdom

[‡]Department of Chemistry, Imperial College London, South Kensington, London SW7 2AZ, United Kingdom

[§]Institute for Chemical and Bioengineering, Department of Chemistry and Applied Biosciences, ETH Zürich, Wolfgang-Pauli-Strasse 10, CH-8093, Zürich, Switzerland

[∥]Faculty of Engineering and the Environment, and [⊥]Institute for Life Sciences, University of Southampton, Southampton, SO17 1BJ, United Kingdom

Supporting Information

ABSTRACT: The ability to miniaturize biochemical assays in water-in-oil emulsion droplets allows a massive scale-down of reaction volumes, so that high-throughput experimentation can be performed more economically and more efficiently. Generating such droplets in compartment-on-demand (COD) platforms is the basis for rapid, automated screening of chemical and biological libraries with minimal volume consumption. Herein, we describe the implementation of such a COD platform to perform high precision nanoliter assays. The coupling of a COD platform to a droplet absorbance detection set-up results in a fully automated analytical system. Michaelis−Menten parameters of 4-nitrophenyl glucopyranoside hydrolysis by sweet almond β-glucosidase can be generated based on 24 time-courses taken at different substrate concentrations with a total volume consumption of only 1.4 μL. Importantly, kinetic parameters can be derived in a fully unsupervised manner within 20 min: droplet production (5 min), initial reading of the droplet sequence (5 min), and droplet fusion to initiate the reaction and read-out over time (10 min). Similarly, the inhibition of the enzymatic reaction by conduritol B epoxide and 1-deoxynojirimycin was measured, and K_i values were determined. In both cases, the kinetic parameters obtained in droplets were identical within error to values obtained in titer plates, despite a >10^4-fold volume reduction, from micro- to nanoliters.

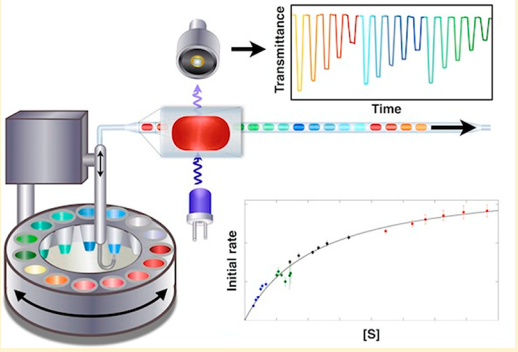

Quantitative assays are at the heart of biological and chemical experimentation. Large numbers of samples must be interrogated when multiparametric spaces are explored combinatorially to identify hits that cannot be rationally predicted, for example, in drug discovery or protein engineering. Miniaturization of sample sizes and automation of handling steps are practical imperatives in making this technology affordable and available to a wider circle of researchers beyond large companies who are not limited by capital expenditure. Microfluidic or lab-on-a-chip technologies have shown their potential in pharmacology, cell biology, and biochemistry.[1−4] More recently, droplet-based microfluidics has become an increasingly powerful tool for reducing and processing reaction volumes ranging from microliters to nano-, pico-, or even femtoliters.[5−15]

Water-in-oil emulsion droplets are generated by mixing an aqueous and oil phase, using mechanical emulsification or, for superior control over droplet size and composition, in microfluidic devices.[16] These microcompartments replace the proverbial test tube (or the more contemporary microwell plate) as reaction vessels. Current droplet formation techniques, typically using flow-focusing devices, allow the generation of very large numbers of droplets at rates in excess of 10 kHz,[17,18] and the setting up of experiments in which large genetically encoded libraries on the order of ∼10^6 members can be analyzed (e.g., in directed evolution).[8,11] However, large numbers of droplets are less useful for experiments in which smaller libraries (e.g., compound repertoires that have orders of magnitude fewer library members as compared to genetically encoded libraries) are used. In these instances, compartment-on-demand (COD) platforms can provide an alternative to bulk or flow-focusing droplet formation, and minimize reagent consumption by sampling material into droplets or plugs at

Received: February 13, 2013
Accepted: April 3, 2013
Published: April 3, 2013

   dx.doi.org/10.1021/ac400480z | *Anal. Chem.* 2013, 85, 4761−4769

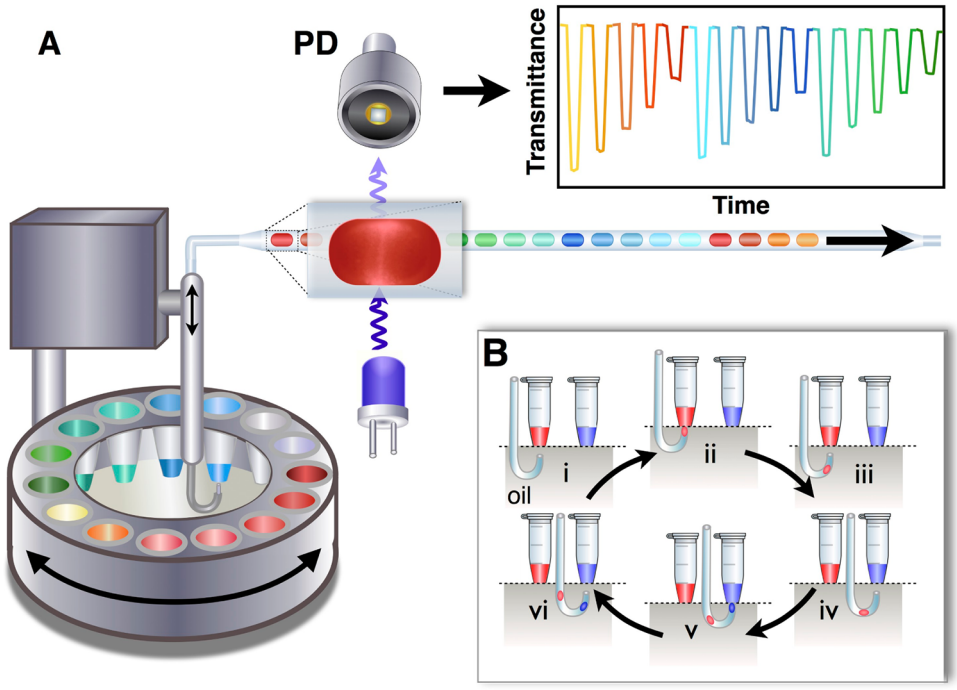

Figure 1. (A) Schematic of the compartment-on-demand platform. Samples (in bottomless tubes) are supplied by rotating an oil-filled carousel. Samples are withdrawn when a sample tube aligns to PTFE tubing located underneath. Negative pressure is applied via a syringe pump operating in continuous withdrawal mode, and droplet compartments are generated by moving the tubing up and down between the carrier phase and the aqueous phase, as shown in (B). The residence time of the hooked end of the tubing in oil or aqueous phase determines the distance between droplets and the droplet volume, respectively. The absorbance of each microdroplet is read by passage between an LED source aligned with a photodetector (PD). A typical data trace is shown in the top right (see Figure 2A) showing absorbance data for droplet sequences with different compounds (corresponding to different colors) and concentration gradients (indicated by shading of each color). (B) Sequential operation of the COD platform. During all steps of operation, the tubing is aspirating liquid at a constant rate. (i) The tip of the tubing is aligned with a given sample. (ii) The tip is lifted so that it sits in the aqueous phase of sample 1 (red). (iii) The tip returns to the oil phase. The change from aqueous to oil phase creates a microcompartment containing a controlled quantity of sample 1 (red). (iv) The tip is aligned below a second sample. (v) The tip is lifted analogously to step (i), but now sample 2 (blue) is taken up. (vi) The tip comes back to the carrier fluid. As a result of the process shown in (B), a sequence of microdroplets with defined contents (sample 1, red; sample 2, blue) emerges in the tubing in a preplanned order. Droplets can be generated at a rate of 0.1−5 s per droplet. No further labeling is necessary as the sequence of sample compartmentalization can be programmed and droplets appear in the tubing as planned. Control over compartment volume and the distance between compartments is exerted by variation of the residence times of the tip in aqueous and oil phases.

significantly lower throughput (1−10 Hz). The lower droplet production rate presents an opportunity to exert full control over the sequence and composition of each compartment. Control over the compartment contents serves as an alternative to encoding so that labeling steps become superfluous and can be used for easy production of segmented concentration gradients. Here, the confidence in the data obtained from each individual droplet is the crucial basis for the reduction of droplet numbers (in turn enabling lower reagent consumption) without loss in information quality.

Several COD platforms have been introduced in the past few years and applied to combinatorial studies.[19,20] On-chip platforms based on valves[21] or high-precision dosing pumps that allow formation of droplets at the junction of multiple inlet ports[20] have been used to generate microliter droplets with highly accurate reagent dispensing to generate concentration gradients of analytes. Other platforms that generate droplets directly from samples in titer plates in specific sequences use valves to dispense these "droplet trains" for incubation, which can be in tubing, or on- chip, and for further analysis.[22] Continuous sampling of a PCR assay has been realized using an automated platform for sample manipulation in which 500 nL droplets were sequentially formed into a droplet train via a dual aspirating valve unit for injection into tubing. Using a commercially available autosampler, kinetic analysis could be performed by drawing samples to form 5 μL droplets, which were then split into smaller droplets and mixed with other assay components to afford final assay droplet volumes of over 800 nL.[23] Such valve systems allow control over the sequence of droplets, but result in large plugs (assay volumes of 800 nL to 5 μL), imply slow droplet generation (up to 30 s for one droplet), and incur a significant risk of sample contamination within the valve itself.

A few platforms generate droplets through the use of negative pressure. For example, the DropLab[24,25] and a study by Wen et al.[26] report the suction of aqueous and oil samples to create concentration gradients via the sequential uptake of the reagent droplets in the low nanoliter range. In the former work with DropLab, reagents are mixed by sucking varying ratios of liquid prior to flow segmentation with oil, whereas the latter study uses merging elements to combine droplets. Although the use of negative pressure eliminates the need for valves and allows formation of much smaller droplets (20 pL to 3 nL), mixing aqueous solutions in the DropLab system leads to potential contamination and the initiation of reactions prior to droplet formation. Conversely, passive on-chip merging allows precise timing of the fusion event, for example, through pillar

dx.doi.org/10.1021/ac400480z | Anal. Chem. 2013, 85, 4761−4769

designs,[27] although these designs restrict to some extent the range of droplet volumes that can be used.

The current work seeks to overcome the technical complexity of previous COD platforms and to maintain a high-quality readout, control key operations robotically, and allow integration with liquid handling system that are commonly used for compound storage and supply. We achieve alternation of droplets and controlled merging without the use of valves, multiple inlets, or a microfluidic chip, with control and flexibility over the content, size, and number of droplets. The processes that have to be precisely controlled are the supply of the compounds tested and their dilution to determine functional data as a basis for structure−activity relationships.

In our COD platform, a robotic sampler generates a sequence of microsegments (at a frequency of 0.2 Hz) and also governs their chemical/biological payload, which can be varied over a series of compartments. A detection module that interrogates droplets traveling inside the tubing to give quantitative absorbance readouts expands the scope of optical analysis beyond fluorescence. Accordingly, the time-dependent variation of absorbance as a result of an enzyme-catalyzed reaction can be determined in a droplet sequence and provides a quantitative read-out for a series of reagent concentrations. Reactions were initiated by passive merging of droplets directly in tubing by acceleration of the flow of droplet pairs placed in close proximity to each other. Time-courses were extracted by moving the train of droplets back and forth through the absorbance detection module. The programmable and robotic control of the COD platform allows the creation of a sequence of microfluidic aqueous segments with defined volumes, frequencies, and interdroplet spacings. High-quality data were obtained for the enzymatic hydrolysis of 4-nitrophenyl glucopyranoside by sweet almond β-glucosidase: time-resolved kinetics for individual droplets with different substrate concentrations were used to derive k_{cat} and K_M values within 20 min in a single run, with full automation from droplet generation to data collection.

RESULTS AND DISCUSSION

A Robotic COD Platform. The COD platform (Figure 1) creates user-defined sequences of droplets with control over content and volume. Specifically, it transforms aqueous samples into individual microcompartments by continuous suction of fluid into PTFE tubing (200 μm ID) from different samples loaded in a carousel. Currently, the minimum sample volume needed to generate droplets is ~20 μL, which provides a layer deep enough for the tubing to be immersed while in the "up" position. To form droplets of a given sample, a solenoid controlling the vertical motion of the end of a section of tubing withdraws either oil or sample (placed in bottomless PCR tubes) from below (Figure 1B), turning the aqueous stream into an alternating sequence of droplets. In the "down" position, the tubing is fully immersed in the oil phase, while in the "up" position, its tip is inside the aqueous phase. The PTFE tubing and the oil phase are matched in their interfacial properties, and so upon retraction from the aqueous sample the tubing is free of any aqueous contamination.

Varying concentration and thus mixing specific volumes of different reagents requires precise control over droplet size in our COD platform. To do so, the size of the droplet (created from the aqueous phase) and the distance between droplets (created by the oil phase) were controlled by varying the residence times in each phase. The size of each microsegment was measured to determine the accuracy of droplet formation, and observed volumes were compared to theoretical volumes (Figure S4, Supporting Information). Relative standard deviations of the droplet lengths were typically less than 10%. This deviation is caused by the inherent pulsing of the syringe pump. For kinetic experiments, the actual sizes of droplets produced were extracted from their "absorbance signature", and these values, rather than the theoretically expected volumes, were used in the determination of kinetic parameters.

Absorbance Measurements. A large number of conventional enzymatic assays rely on UV−Vis spectrophotometric detection of a chromophore-containing product. Unfortunately, miniaturization of optical path-lengths results in decreased absorbance in accordance with the Beer−Lambert law. This is not a limitation for fluorescence-based measurements, and thus absorbance detection has only been used sparingly in microfluidic assays. Examples of such studies include a coupled assay to measure alcohol oxidation kinetics using disc microfluidics with a 10 mm path length,[28] glucose detection through a 475 μm-long droplet,[29] pH sensing by recording absorbance movies through a 27 μm optical path,[30] and dye calibration through 500 μm diameter tubing.[20] As in the latter reference, we have implemented absorbance-based detection using a custom-made polymeric holder that serves to align the light source and detectors accurately across the tubing. This configuration bypasses the need for microfluidic chips in which fibers are embedded[31] and provides a simple solution for optical detection. A typical read-out is shown in Figure 2A. Fiber core sizes were assessed for their signal-to-noise ratio, with the optimal design having a core diameter of 200 and 50 μm for connection to the light source and the detector, respectively. These fiber sizes were used for all subsequent experiments unless stated otherwise.

On the basis of a typical reading (as shown in Figure 2A), both the residence time and the average absorbance for each droplet can be retrieved by postprocessing raw data. On the basis of the known flow rate, the residence time of a given droplet across the detection zone can be converted into a volume (Figure S4). Droplet size was determined using the edge effects for solutions of low absorbance. In addition, the average transmittance for PBS buffer alone is higher than the base transmittance through the oil and was therefore used as a blank for correction of the absorbance baseline. To assess the sensitivity and limit of detection of the described implementation, dilutions of 4-nitrophenol were pipetted into the loading tubes and transformed into microsegments. Five readings were taken for each condition and averaged. The absorbance read-out (Figure 2B) shows excellent linearity (R^2 of 0.99) as a function of dye concentration with a concentration detection limit approximately 3 μM of 4-nitrophenol (corresponding to three standard deviations of the background noise). This compares favorably with other embodiments of absorbance detection in microfluidic systems (e.g., 13 μM with a 28 μm path length)[32] and, for the assay presented herein, is more than sufficient to extract quantitative information (from enzyme turnovers that give rise to product concentrations in the micromolar to millimolar range).

Creation of Linear Gradients. The creation of controlled dilution gradients is crucial when performing quantitative assays that provide accurate enzyme kinetic data for subsequent structure−activity relationships. To generate linear concentration gradients, microdroplet pairs were generated at a low flow rate (10−20 nL/s) with the first droplet being smaller than

dx.doi.org/10.1021/ac400480z | Anal. Chem. 2013, 85, 4761−4769

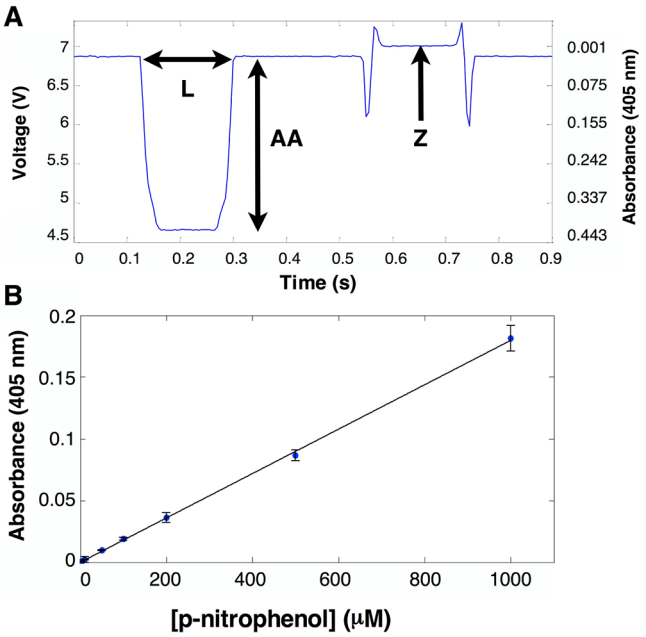

Figure 2. (A) Quantifying absorbance in droplets. A typical trace of an absorbance read-out ($A^{405\ nm}$) for two droplets (representing sample-loaded and empty compartments) flowing through a PTFE tubing (200 μm diameter). The first signal refers to a droplet containing 4-nitrophenol (2 mM) in PBS buffer, and the second containing buffer only. Each droplet was interrogated with an LED source with a peak emission at 405 nm. *L* defines the residence time of the droplet in the detection zone and corresponds to the length of the droplet. *AA* is the average absorbance of the droplet contents. The recovered signal for buffer droplets corresponded to the highest voltage and was defined as zero absorbance (*Z*). In this example, the continuous oil phase had an absorbance $A^{405\ nm}$ of approximately 0.02. The signal spikes (at the droplet extremities) are a result of edge effects that are brought about by refractive index changes between the aqueous and oil phases. (B) Calibration of the absorbance detection with 4-nitrophenol. Premade dilutions were introduced into the loading tubes of the carousel, and the droplet absorbance was read for each condition (n = 5). The data correlate linearly (R^2 of 0.99), and the detection limit (three standard deviations above the background noise) suggests that measurements down to 3 μM 4-nitrophenol are possible.

the following droplet and separated by a short oil plug. Once all of the droplet pairs were produced, the flow was halted and then accelerated to a flow rate of 300 nL/s. This resulted in paired droplets getting closer to each other, due to an imbalance of oil leaking through the corner gutters of both droplets, which behave as leaky pistons.[19,20,33] The size of the oil plug between the two droplets gradually decreased until the continuous phase completely drains and droplets were able to coalesce. This process was visualized and is detailed in the Supporting Information (Figure S5).

By programming the frequency of the up/down motion of the solenoid, droplet pairs of different size ratios were generated. Linear gradients were automatically created so that each droplet pair corresponded to a unique size combination. The total volume of the merged pairs was kept constant at approximately 60 nL. In this setup, the time taken to create a droplet was 0.1−5 s (representing >10-fold faster droplet generation as compared to DropLab[24,25]). Using the software controlling the COD platform, automated generation of 50 droplet pairs and subsequent merging in tubing was shown (see Figures S7, S8, Supporting Information). Every droplet pair successfully merged. The parameters for merging were examined and showed a dependence on the volume of the oil plug separating droplet pairs with optimal fusion at minimum oil volume (<5 nL). Moreover, the range over which a concentration gradient can be produced is defined by the size ratio between the smaller first droplet and the larger second droplet. In the current studies, the largest dilution ratio used was 1:5 with a volume of the smallest droplet of 10 nL. Finally, it should be noted that the frequently employed method of serial dilution, that is, multiple sequential dilution steps by the same factor, makes it hard to obtain as good coverage of a concentration range as in Figure 3C, which in turn often precludes acquisition of data good enough for quantitative analysis in structure−activity relationships.

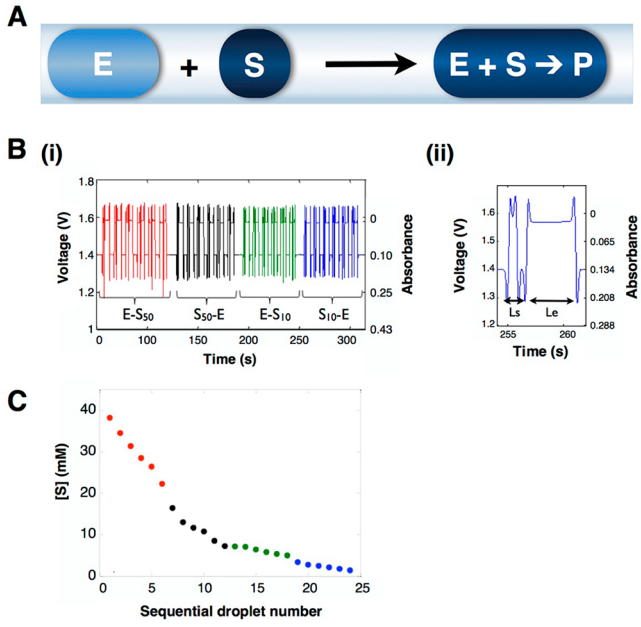

Figure 3. (A) Merging scheme for a pair of microdroplets inside tubing. A large compartment loaded with enzyme (E) will catch up with a smaller compartment loaded with substrate (S) placed immediately in front of it. Merging triggers the hydrolytic reaction leading to the formation of product P (monitored at 405 nm). (B) Confirmation and sizing of the droplet sequence. (i) Four sets of six droplet pairs of enzyme (E) and substrate (10 and 50 mM, referred to as S_{10} and S_{50}, respectively) of varying sizes were produced. (ii) The enzyme/substrate droplets were analyzed shortly after generation, and prior to merging, to determine the precise size of each droplet. Sizes were measured by determining the distances L_s (length of the substrate droplet) and L_e (length of the enzyme droplet) as described previously. The illumination source was a cold white LED, and the fiber core sizes for illumination and detection were 100 and 50 μm, respectively. (C) Automated concentration gradient. The substrate concentration range after mixing of all droplet pairs was 1.3−38.2 mM. The color code relates the data points in (C) to the primary data in (B)(i).

Programmed Automation. All of the steps including droplet formation, confirmation and sizing of the droplet sequence, triggering of the merging, and back and forth measurement were implemented in a single program. The schematic of the program is shown in Figure 4.

Enzyme Kinetics in Droplets. The hydrolysis of the chromogenic substrate 4-nitrophenyl glucopyranoside by sweet almond β-glucosidase was chosen as a model reaction for

dx.doi.org/10.1021/ac400480z | *Anal. Chem.* 2013, 85, 4761−4769

Figure 4. The automated workflow programmed to run kinetic assays. Schematic diagram of the four steps that provide a full set of Michaelis–Menten data: (1) loading of the droplet pairs corresponding to different points of the Michaelis–Menten plot; (2) confirming and sizing of the droplet pairs prior to fusion; (3) droplet merging in tubing initiates the reaction; and (4) droplets are moved back and forth for reading of the reaction progress by absorbance. Such readings can be repeated many times until the reaction has advanced sufficiently to describe a full time-course. The ability to carry out as many measurements as necessary makes this system amenable to most reactions (with time scales from a minute to several hours or more). The sizing data (step 2) and the data for the time-courses (step 4) were stored in individual files. This process can be repeated for multiple samples that are sequentially supplied from the carousel of the robotic sampler (Figure 1A).

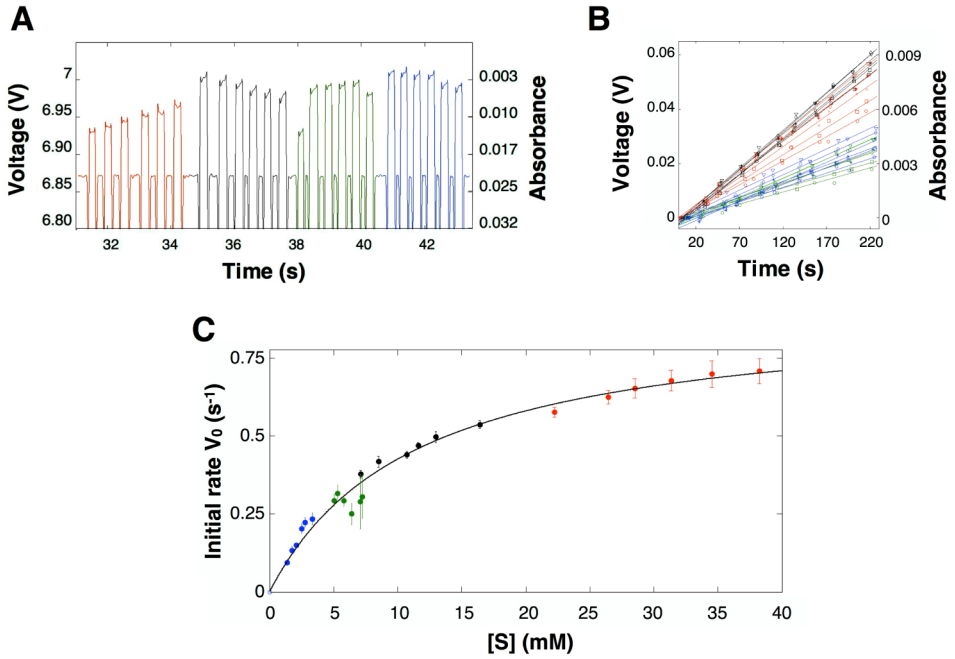

Figure 5. Derivation of Michaelis–Menten plots from primary data. (A) Confirmation of fusion of droplet pairs and initial assay reading. The first data point was measured 30 s after initiating the acceleration to cause merging. The LED used for these absorbance measurements emitted at 405 nm. The color code corresponds to the same data points as in Figure 3. (B) Time-resolved measurements of average absorbance value for each assay point, with corresponding linear fits superimposed. Initial readings were set to zero volts to highlight the diversity of slopes. The color code corresponds to the droplets displayed in Figures 3B,C and 4A. (C) Michaelis–Menten plot based on 24 substrate concentrations extracted from the data in (A) and (B). The values for V_o are obtained by converting the voltage change per time into a concentration change per time and then dividing these values by the enzyme concentration. Colors correspond to the dilution set of Figure 3 and groups of initial rates in Figure 4B. Error bars shown represent the error in the linear fits shown in Figure 4B.

monitoring the action of a typical hydrolytic enzyme and deriving Michaelis–Menten parameters. Reaction rates with a range of substrate concentrations were followed over time, and initial rates, V_o, were determined. Each substrate concentration corresponds to a combination of enzyme and substrate samples that are fused in different volume ratios. Two substrate stock concentrations (10 and 50 mM that are diluted in ratios up to 1:5) were needed to generate a substrate concentration range between 2 and 40 mM (see Figure 3). These stock solutions and an enzyme stock (at 78 nM) were loaded in three adjacent wells in the carousel (Figure 1) and used to generate pairs of droplets containing enzyme and substrate (Figure 3A). Once all of the pairs were loaded in sequence, merging was triggered. The first reading was taken after approximately 30 s (as shown in Figure 5A). To precisely account for size variation and confirm that the planned sequence of droplets was indeed generated, an absorbance detection system was positioned close to the site of droplet formation to monitor droplet lengths, which in turn were used to derive the precise enzyme and substrate concentration for each mixture. This initial reading is shown in Figure 3B(i), and an expansion showing a single droplet pair is shown in Figure 3B(ii). The resulting screening range for substrate concentration is displayed in Figure 3C.

For measuring further time points, two marker droplets (containing 1 mM 4-nitrophenol) loaded at the front and the rear of the sequence trigger the automated reversal of the flow direction. Consequently, the droplet sequence flowed back and forth passing the absorbance reader. Absorbance measurements for individual droplets were recorded for each passage through the detector (Figure S9). These time points were then assembled into time-courses (Figure 5B) for each droplet in the known sequence (Figure 5B).

On the basis of the accurate size information for the substrate and enzyme droplets, the true concentrations of enzyme and substrate in each reaction droplet were determined and used to convert the initial rate data shown in Figure 5B into a

dx.doi.org/10.1021/ac400480z | Anal. Chem. 2013, 85, 4761–4769

Michaelis–Menten plot as shown in Figure 5C. It was found that in the droplets a background reaction of spontaneous substrate hydrolysis (at the oil/water interface) gave rise to a linear increase in product concentration (Figure S10). Accordingly, the initial slopes were corrected for spontaneous hydrolysis before conversion to turnover numbers. The data obtained were modeled with the Michaelis–Menten equation yielding the kinetic parameters of K_M = 11.4 ± 2 mM and k_{cat} = 0.9 ± 0.2 s^{-1}. These values are in close correspondence with those determined in a microtiter plate (K_M = 12.8 ± 4 mM and k_{cat} = 1.3 ± 0.3 s^{-1} (shown in Figure S11)). The total volume necessary to describe a Michaelis–Menten plot was 720 nL of enzyme stock and 360 nL for each substrate stock solution (50 and 10 mM).

Inhibition. Our approach was subsequently extended to a ternary combination of reagents and exemplified with inhibition studies for a known inhibitor of β-glucosidase, 1-deoxynojirimycin hydrochloride (DNM).[34] To obtain Michaelis–Menten kinetic plots in the presence of the inhibitor, different concentrations of inhibitor and substrate were pipetted into the loading tubes. Drawing samples from these stocks allowed easy screening of inhibitor concentrations spanning 3 orders of magnitude and demonstrated full use of all 15 loading slots in the current carousel. Here, triplets were created to combine enzyme, substrate, and inhibitor with the final substrate droplet representing 50% of the final volume to ensure reproducible merging of the triplets. A schematic for triplet droplet merging is shown in Figure 6A. Michaelis–Menten plots for different inhibitor concentrations are shown in Figure 6B.

Subsequently, rates in the presence of a fixed substrate concentration and varying concentrations of DNM and Conduritol B Epoxide (CBE) were measured. We followed inhibition at high substrate concentrations (23 mM) to maximize product formation. The ratio between the maximum initial rate (with no inhibitor) and the initial rate at different inhibitor concentrations is represented in Figure 6C.

From these data, the IC_{50} for DNM was determined to be 108 ± 40 μM by fitting to eq 1:[35]

$$\frac{V_0}{V_0^{\max}} = \frac{1}{1 + \frac{[I]}{IC_{50}}} \quad (1)$$

This inhibition constant corresponds to an approximate K_i value of 36 μM, assuming competitive inhibition and using the Cheng–Prusoff equation.[36] This correlates well with the literature value for K_i of 47 μM.[34] The data set for CBE cannot be used for fitting because CBE is an irreversible inhibitor, but the observed inhibition is consistent with microtiter plate readings (cf., Figure S13).[37]

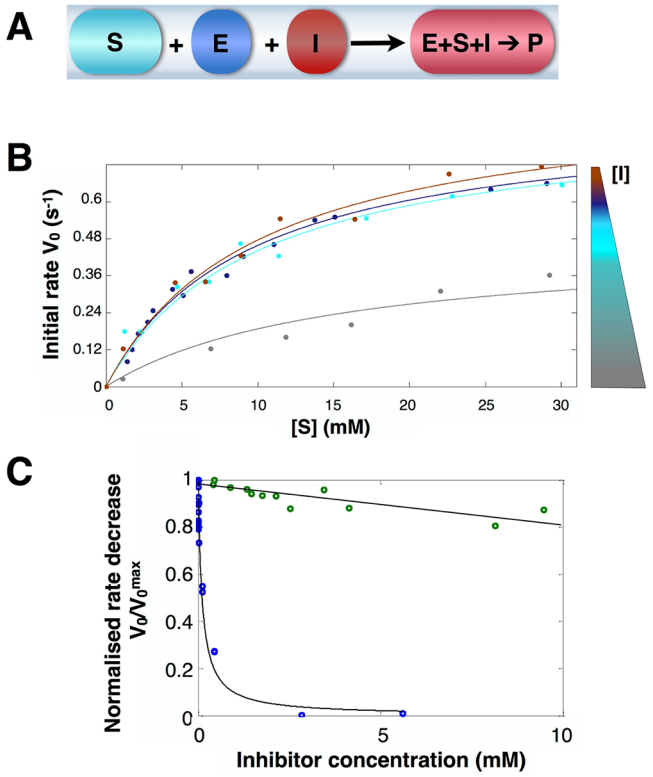

Figure 6. Determination of inhibition kinetics. (A) Schematic for triplet droplet merging. (B) Michaelis–Menten plot in the presence of selected concentrations of 1-deoxynojirimycin hydrochloride (DNM). The final concentrations of inhibitors were 200 μM (dark gray), 20 nM (cyan), 200 pM (brown), and 0 nM (purple). Here, enzyme concentration was fixed at 16.5 nM. (C) Normalized rate change V_0/V_0^{max} versus inhibitor concentration for DNM (blue dots) and CBE (green dots). The data points for DNM were fitted to generate an IC_{50} (see text for details). For CBE a line was drawn merely to guide the eye. Conditions: [E] = 19 nM; [S] = 23 mM; [PBS] = 100 mM (pH 7.4).

IMPLICATIONS AND CONCLUSIONS

Miniaturization. The COD platform can perform automated enzyme kinetic experiments without supervision and generate data comparable in quality to microtiter plate readings, but works with much smaller quantities of reagents (e.g., 720 nL of enzyme vs 240 μL in a 96-well plate for 24 data points). Our COD platform also compares favorably with other COD platforms used for kinetic assays. For example, although the DropLab[24,25] system has been claimed to operate with 2 nL per reaction (although larger droplets are typically displayed in ref 24) and previously described valve systems[23] consume 188 nL of enzyme per data point, the current COD platform uses an average of 30 nL of enzyme per data point. Miller et al.[35] successfully carried out a screen of small molecule enzyme inhibitors in 140 pL droplets. However, the confidence in the data obtained from each single droplet measurement was so low that more than 10 000 data points were needed to a construct a reliable binding curve.[35] Massive statistical averaging allowed quantitative interpretation of a scattered data set to obtain an IC_{50} value. Our COD system takes the completely different approach of maximizing the information extracted per unit volume, so that 500-times fewer data points are needed. Precise control over droplet size and derivation of time-courses (rather than single point assays) are responsible for data quality being equivalent to cuvette or microplate experiments. This increase in data quality is obtained at the price of a 5000-fold larger droplet volume (720 nL vs 140 pL), so that the approach of Miller et al. consumes on balance about 10-times less reagent to obtain a binding curve. When minimization of reagent consumption is key, this system will be preferred. Nevertheless, when single species, such as cells,[38−40] of limited availability are to be interrogated (so that the number of droplets determines their consumption) and time-dependent data must be obtained, then the current COD platform becomes the method of choice. Furthermore, the larger volumes of COD platforms allow absorbance measurements for which the light path in smaller droplets is too short, enabling a range of assays for which there are no convenient

dx.doi.org/10.1021/ac400480z | Anal. Chem. 2013, 85, 4761−4769

fluorescence-based alternatives. Regardless, each of the above platforms has obvious advantages as compared to typical kinetic assays in titer-plates: (i) more data points can be obtained with less reagent (in our case, the volume reduction from microliter to nanoliter is in excess of 10^4-fold), (ii) fewer pipetting steps (20 times fewer for the data shown in this work) are needed as they are replaced by automated volume calculations and liquid handling without the expense that industrial facilities attract in capital expenditure and maintenance; and (iii) single species experiments can be carried out with data quality that is of quality similar to that of normal large-scale experiments.

Spatial Encoding. Previous droplet screening systems have frequently made use of dyes that provided information about the concentration and/or identity of the contents of the droplet.[23,35,38,41,42] By contrast, no labels are needed in the described platform, because the sequence of droplets is entirely programmable. Once the sequence is set, only simple back-and-forth movements are necessary for detection with no disturbance in droplet order being observed. The approach of sequential encoding greatly reduces the technical complexity of the assay and obviates the need for multiple detection schemes. Ultimately, reliance on coding dyes will limit the numbers of compounds that can be screened because there are a finite number of available dyes that can be optically distinguished. Before our COD system described here can be applied to a combinatorial screen, further engineering of the compound supply (via the carousel and its integration with conventional liquid handling systems) will be necessary to carry out automated large-scale experiments.

Droplet Handling without Chips. Performing the entire assay within tubing eliminates problems tied to integration of droplet generation and handling in microfluidic chips, such as the stability of droplet generation or insertion of a sequence of "droplet trains" through valves. No chips had to be designed and fabricated for this study, although our system can be easily integrated with chips while maintaining a specific droplet sequence, if desired.[26] The program that controls robotic droplet formation is readily adjusted to set the number and size of the droplets to be merged. Moreover, this work establishes a new method to merge droplets by exploiting hydrodynamic flow properties that lead to droplet fusion based on size difference and does not require additional features provided in planar chip formats. Relying on full control over droplet size allows the on-demand generation of varied concentrations of droplet contents. In the inhibition screen, we describe how we merged three droplets with premixed inhibitor concentrations to demonstrate full use of all wells available in the carousel. However, quadruplet combinations of enzyme, substrate, inhibitor, and buffer could be merged to create inhibitor dilutions in a fully automated fashion.

Kinetic Studies in Droplets. Several other droplet systems have previously been used to measure kinetics, but crucial differences exist. Song et al.[43] demonstrated how control over the flow rates of the different fluid inlets in a flow-focusing device can be used to measure fast enzyme kinetics. To obtain kinetic data with sufficient quality, a dilution stream was imaged at nine points along the channel with distance corresponding to the reaction time. Historically, bar a few exceptions,[44−46] most studies in droplets have derived kinetic information from end-point detection, because series of droplets created at high-throughput cannot easily be kept in sequence. In these cases, following a specific droplet over time becomes difficult (especially when large numbers of repeats are required to improve data quality). For example, in experiments employing the DropLab,[24,25] only one measurement of product concentration was taken (instead of following reaction turnover as a function of time), and this one-point measurement provided the input for a plot that shows the "rate" decrease as a function of inhibitor concentration. Measuring just one time point to derive an initial rate is based on the assumption of linearity, which is only correct when early phases of time-courses are captured. By contrast, a concentration gradient that is interrogated during each back-and-forth movement gives access to full time-course measurements for the same droplet, improves data quality (by a suitable curve fit through multiple data points, as in Figure 5B), and allows ready identification of nonlinearity. The ability to measure absorbance in our format further increases the versatility of this setup, because the circle of assays is increased beyond fluorescence that has been the sole readout in previous platforms.[24,25]

Outlook. Future challenges will focus on the integration of this COD platform with analytical interfaces, to extend compound delivery to multistep processes, and to address biological experiments that cannot be performed in bulk. Interfacing with separation techniques such as capillary electrophoresis[47] or analysis by mass spectroscopy[48] will allow a high number of experiments to be examined sequentially and with minimum supervision. Cell culturing can also be performed on chip and integrated with droplet formation.[49−51] Sequential robotic delivery of reagents is important, for example, in ELISA assays[52] or other types of immunoassays and can be programmed into the workflow of this COD platform. When concentration gradients are set up for droplets containing single cells or clusters of a few cells that can be supplied in defined concentrations via Poisson distribution, quantitative time-dependent experiments will be carried out on small populations.[53] Such an approach would allow the revalidation of data from microplate cell-based assays that are only possible with potentially heterogeneous cell populations.[54,55]

EXPERIMENTAL SECTION

Droplet Generation and Merging. The carousel was filled with perfluorinated oil (60 mL, FC-40), mixed with perfluorooctanol (PFO; 0.5%, v/v; Sigma-Aldrich). Samples were supplied from a carousel that carried up to 15 samples sitting on a metal ring with 15 holes holding PCR tubes (Molecular BioProducts, 0.2 mL) that had the bottom 2 mm sliced off. To generate droplets, PTFE tubing (Ultramicrobore, 0.2 mm ID, 0.4 mm OD, Cole Parmer) was guided by a stainless steel hook to suck the samples from below (see Figure S1). To allow digital positioning, the carousel was mounted onto a stepper-motor allowing precise alignment of the tubing and sample. Negative pressure was applied from a glass syringe (200 μL) with a syringe pump operating in withdrawal mode at constant debit (Chemyx, Fusion 200). Both solenoid and stepper motor were controlled by a custom-written Labview program. In a typical experiment, 20−30 droplets were injected over a distance of 15 cm from the first to last droplet. The droplet volume was adjusted by variation of the suction flow rate (originating from the pump) and the dwell time of the tubing in the aqueous phase (see Figure S4). The Labview program also controlled merging of droplet pairs and the back-and-forth flow direction changes for the detection of absorbance over time.

dx.doi.org/10.1021/ac400480z | Anal. Chem. 2013, 85, 4761−4769

Absorbance Measurements. The tubing was aligned with respect to the fibers via a custom-made polymeric block made of black acetal. An analog-to-digital board (National Instruments) was used to read voltages from the photodetector. Typical absorbance readings were taken with a reading rate of 200 Hz using a custom-written Labview program. A low-pass filter (with a high frequency cutoff at 30 Hz) was applied to all readings. Using a molar extinction coefficient ($\varepsilon^{405\ nm}$) of 13 200 M^{-1} cm^{-1} for 4-nitrophenol in PBS, measured in a 1 cm path length quartz cuvette, the effective average path length through the droplets was calculated as 151 μm. This value is consistent with the tube diameter of 200 μm and confirms good alignment of the tubing and fibers.

■ ASSOCIATED CONTENT

Supporting Information

Technical details describing droplet formation, control of droplet size and merging, as well as comparison of kinetics with microtiter plate data. Videos are also supplied. This material is available free of charge via the Internet at http://pubs.acs.org.

■ AUTHOR INFORMATION

Corresponding Authors

*E-mail: x.niu@soton.ac.uk.
*E-mail: andrew.demello@chem.ethz.ch.
*E-mail: fh111@cam.ac.uk.

Notes

The authors declare the following competing financial interest(s): Several authors are co-founders of a droplet microfluidics company, Drop-Tech, F.G., L.V., B.T.K., J.B.E., X.N., A.J.d.M., and F.H.

■ ACKNOWLEDGMENTS

This research was funded by the European Research Council and the EPSRC. S.R.A.D. and M.F. were supported by EU Marie-Curie fellowships. F.H. and J.B.L are ERC Starting Investigators. L.V. was supported by a BBSRC Enterprise fellowship. We thank Maren Butz for useful discussions and comments.

■ REFERENCES

(1) Hong, J.; Edel, J. B.; Demello, A. J. *Drug Discovery Today* **2009**, *14*, 134−146.
(2) Neužil, P.; Giselbrecht, S.; Länge, K.; Huang, T. J.; Manz, A. *Nat. Rev. Drug Discovery* **2012**, *11*, 620−632.
(3) Kang, L.; Chung, B. G.; Langer, R.; Khademhosseini, A. *Drug Discovery Today* **2008**, *13*, 1−13.
(4) Paul, S. M.; Mytelka, D. S.; Dunwiddie, C. T.; Persinger, C. C.; Munos, B. H.; Lindborg, S. R.; Schacht, A. L. *Nat. Rev. Drug Discovery* **2010**, *9*, 203−214.
(5) Theberge, A. B.; Courtois, F.; Schaerli, Y.; Fischlechner, M.; Abell, C.; Hollfelder, F.; Huck, W. T. S. *Angew. Chem., Int. Ed.* **2010**, *49*, 5846−5868.
(6) Huebner, A. M.; Abell, C.; Huck, W. T. S.; Baroud, C. N.; Hollfelder, F. *Anal. Chem.* **2011**, *83*, 1462−1468.
(7) Schaerli, Y.; Hollfelder, F. *Mol. BioSyst.* **2009**, *5*, 1392−1404.
(8) Agresti, J. J.; Antipov, E.; Abate, A. R.; Ahn, K.; Rowat, A. C.; Baret, J. C.; Marquez, M.; Klibanov, A. M.; Griffiths, A. D.; Weitz, D. A. *Proc. Natl. Acad. Sci. U.S.A.* **2010**, *107*, 4004−4009.
(9) Teh, S.-Y.; Lin, R.; Hung, L.-H.; Lee, A. P. *Lab Chip* **2008**, *8*, 198−220.
(10) Casadevall i Solvas, X.; Niu, X.; Leeper, K.; Cho, S.; Chang, S.-I.; Edel, J. B.; Demello, A. J. *J. Visualized Exp.* **2011**, *58*, e3437.
(11) Kintses, B.; van Vliet, L. D.; Devenish, S. R. A.; Hollfelder, F. *Curr. Opin. Chem. Biol.* **2010**, *14*, 548−555.
(12) Vyawahare, S.; Griffiths, A. D.; Merten, C. A. *Chem. Biol.* **2010**, *17*, 1052−1065.
(13) Guo, M. T.; Rotem, A.; Heyman, J. A.; Weitz, D. A. *Lab Chip* **2012**, *12*, 2146−2155.
(14) Kintses, B.; Hein, C.; Mohamed, M. F.; Fischlechner, M.; Courtois, F.; Lainé, C.; Hollfelder, F. *Chem. Biol.* **2012**, *19*, 1001−1009.
(15) Wootton, R. C. R.; Demello, A. J. *Nature* **2012**, *483*, 43−44.
(16) Devenish, S. R. A.; Kaltenbach, M.; Fischlechner, M.; Hollfelder, F. Protein Nanotechnology: Protocols, Instrumentation and Applications. In *Methods in Molecular Biology*, 2nd ed.; Gerrard, J., Ed.; Humana Press: Totowa, NJ, 2013; Vol. *996*, pp 269−86.
(17) Umbanhowar, P. B.; Prasad, V.; Weitz, D. A. *Anal. Chem.* **2000**, *16*, 347−351.
(18) Garstecki, P.; Gitlin, I.; DiLuzio, W.; Whitesides, G. M.; Kumacheva, E.; Stone, H. A. *Appl. Phys. Lett.* **2004**, *85*, 2649.
(19) Churski, K.; Korczyk, P.; Garstecki, P. *Lab Chip* **2010**, *10*, 816.
(20) Cao, J. L.; Kursten, D.; Schneider, S.; Knauer, A.; Gunther, P. M.; Kohler, J. M. *Lab Chip* **2012**, *12*, 474−484.
(21) Churski, K.; Michalski, J.; Garstecki, P. *Lab Chip* **2010**, *10*, 512−518.
(22) Chabert, M.; Dorfman, K. D.; de Cremoux, P.; Roeraade, J.; Viovy, J.-L. *Anal. Chem.* **2006**, *78*, 7722−7728.
(23) Clausell-Tormos, J.; Griffiths, A. D.; Merten, C. A. *Lab Chip* **2010**, *10*, 1302−1307.
(24) Du, W.-B.; Sun, M.; Gu, S.-Q.; Zhu, Y.; Fang, Q. *Anal. Chem.* **2010**, *82*, 9941−9947.
(25) Gu, S.-Q.; Zhang, Y.-X.; Zhu, Y.; Du, W.-B.; Yao, B.; Fang, Q. *Anal. Chem.* **2011**, *83*, 7570−7576.
(26) Wu, J.; Zhang, M.; Li, X.; Wen, W. *Anal. Chem.* **2012**, *84*, 9689−9693.
(27) Niu, X.; Gielen, F.; Demello, A. J.; Edel, J. B. *Anal. Chem.* **2009**, *81*, 7321−7325.
(28) Steigert, J.; Grumann, M.; Brenner, T.; Riegger, L.; Harter, J.; Zengerle, R.; Ducrée, J. *Lab Chip* **2006**, *6*, 1040−1044.
(29) Srinivasan, V.; Pamula, V. K.; Fair, R. B. *Anal. Chim. Acta* **2004**, *507*, 145−150.
(30) Deal, K. S.; Easley, C. J. *Anal. Chem.* **2012**, *84*, 1510−1516.
(31) Zhang, L.; Wang, P.; Xiao, Y.; Yu, H.; Tong, L. *Lab Chip* **2011**, *11*, 3720−3724.
(32) Song, W.; Yang, J. *Lab Chip* **2012**, *12*, 1251−1254.
(33) Baroud, C. N.; Gallaire, F.; Dangla, R. *Lab Chip* **2010**, *10*, 2032−2045.
(34) Schuster, M. *Bioorg. Med. Chem. Lett.* **1999**, *9*, 615−618.
(35) Miller, O. J.; El-Harrak, A.; Mangeat, T.; Baret, J. C.; Frenz, L.; Debs, El, B.; Mayot, E.; Samuels, M. L.; Rooney, E. K.; Dieu, P.; Galvan, M.; Link, D. R.; Griffiths, A. D. *Proc. Natl. Acad. Sci. U.S.A.* **2012**, *109*, 378−383.
(36) Yung-Chi, C.; Prusoff, W. H. *Biochem. Pharmacol.* **1973**, *22*, 3099−3108.
(37) Falshaw, A.; Hart, J. B.; Tyler, P. C. *Carbohydr. Res.* **2000**, *329*, 301−308.
(38) Brouzes, E.; Medkova, M.; Savenelli, N.; Marran, D.; Twardowski, M.; Hutchison, J. B.; Rothberg, J. M.; Link, D. R.; Perrimon, N.; Samuels, M. L. *Proc. Natl. Acad. Sci. U.S.A.* **2009**, *106*, 14195−14200.
(39) Huebner, A.; Olguin, L. F.; Bratton, D.; Whyte, G.; Huck, W. T. S.; de Mello, A. J.; Edel, J. B.; Abell, C.; Hollfelder, F. *Anal. Chem.* **2008**, *80*, 3890−3896.
(40) Shim, J.-U.; Olguin, L. F.; Whyte, G.; Scott, D.; Babtie, A.; Abell, C.; Huck, W. T. S.; Hollfelder, F. *Anal. Chem.* **2009**, *131*, 15251−15256.
(41) Cai, L. F.; Zhu, Y.; Du, G. S.; Fang, Q. *Anal. Chem.* **2012**, *84*, 446−452.
(42) Pregibon, D. C.; Toner, M.; Doyle, P. S. *Science* **2007**, *315*, 1393−1396.

(43) Song, H.; Ismagilov, R. F. *J. Am. Chem. Soc.* **2003**, *125*, 14613−14619.
(44) Huebner, A.; Bratton, D.; Whyte, G.; Yang, M.; Demello, A. J.; Abell, C.; Hollfelder, F. *Lab Chip* **2009**, *9*, 692−698.
(45) Bui, M.-P. N.; Li, C. A.; Han, K. N.; Choo, J.; Lee, E. K.; Seong, G. H. *Anal. Chem.* **2011**, *83*, 1603−1608.
(46) Fradet, E.; McDougall, C.; Abbyad, P.; Dangla, R.; McGloin, D.; Baroud, C. N. *Lab Chip* **2011**, *11*, 4228−4234.
(47) Niu, X. Z.; Zhang, B.; Marszalek, R. T.; Ces, O.; Edel, J. B.; Klug, D. R.; deMello, A. J. *Chem. Commun.* **2009**, 6159−6161.
(48) Küster, S. K.; Fagerer, S. R.; Verboket, P. E.; Eyer, K.; Jefimovs, K.; Zenobi, R.; Dittrich, P. S. *Anal. Chem.* **2013**, *85*, 1285−1280.
(49) Barbulovic-Nad, I.; Au, S. H.; Wheeler, A. R. *Lab Chip* **2010**, *10*, 1536−1542.
(50) Hufnagel, H.; Huebner, A.; Gülch, C.; Güse, K.; Abell, C.; Hollfelder, F. *Lab Chip* **2009**, *9*, 1576−1582.
(51) Nevill, J. T.; Cooper, R.; Dueck, M.; Breslauer, D. N.; Lee, L. P. *Lab Chip* **2007**, *7*, 1689−1695.
(52) Ali-Cherif, A.; Begolo, S.; Descroix, S.; Viovy, J.-L.; Malaquin, L. *Angew. Chem., Int. Ed.* **2012**, *51*, 10765−10769.
(53) Spiller, D. G.; Wood, C. D.; Rand, D. A.; White, M. R. H. *Nature* **2010**, *465*, 736−745.
(54) Nolan, G. P. *Nat. Rev. Drug Discovery* **2007**, *3*, 187−191.
(55) Tischler, J.; Surani, M. A. *Curr. Opin. Biotechnol.* **2013**, *24*, 69−78.

dx.doi.org/10.1021/ac400480z | *Anal. Chem.* 2013, 85, 4761−4769